Korean J. Chem. Eng., **16**(1), 12-21 (1999)

NUMERICAL ANALYSIS OF LPCVD OF SiO_2 FILMS FROM DIETHYLSILANE/OXYGEN

Eui Jung Kim†, Chul Jin Kim and Kun Yong Chung*

School of Chemical Engineering, University of Ulsan, San 29, Moogeodong, Namku, Ulsan 680-749, Korea
*Department of Chemical Engineering, Seoul National University of Technology, 172 Gongneungdong, Nowonku, Seoul 139-242, Korea
(*Received 4 November 1997 • accepted 13 October 1998*)

Abstract – A mathematical model has been developed to explore the low pressure chemical vapor deposition (LPCVD) of silicon dioxide from diethylsilane (DES)/oxygen in a horizontal hot-wall reactor. We propose a new kinetic mechanism that includes realistic gas-phase and surface reactions. The partial differential equations in two-dimensional cylindrical coordinates are solved numerically by a control-volume-based finite difference method. The model successfully describes the behavior of the experimental data. Film growth rate and uniformity are studied over a wide range of operating conditions including deposition temperature, pressure, reactant flow rate, and distance between the inlet and the wafer. The predicted results show that parasitic gas-phase reactions become significant at higher pressures and temperatures resulting in a decrease in deposition rate. It is seen that the deposition rate becomes a maximum at the O_2/DES ratio of around 2.5. A temperature of 475 °C, a pressure of 0.75 torr, and a total flow rate of 1,000 sccm are found to be desirable for obtaining both high deposition rate and good film uniformity.

Key words: LPCVD, SiO_2 Film, Diethylsilane, Low Temperature Deposition

INTRODUCTION

As current trends in high performance integrated circuits tend toward increasing levels of integration for interconnect technology, low temperature deposition of dielectric films is becoming increasingly important. If one chooses aluminum as an interconnection metal, the dielectric film deposition temperature must be less than 500 °C because of hillock growth on aluminum surfaces leading to fatal device reliability problems. Silicon dioxide films have been widely employed as interlayer dielectrics due to their superior chemical and electrical properties. Further, silicon dioxide films produced by chemical vapor deposition have excellent conformality over severe topography.

Organosilicon materials such as tetraethoxysilane (TEOS), ethyltriethoxysilane (ETOS), diacetoxy-ditertiary butoxysilane (DADBS) and tetramethylcyclotetra-siloxane (TMCTS) have been studied as silicon sources to form silicon dioxide for microelectronics applications. Desirable aspects of these liquid sources are safety and ease of handling relative to silane. However, higher temperatures above 600 °C that are beyond the melting point of aluminum are necessary to produce SiO_2 films for the above source materials. SiO_2 films can be deposited at low temperatures below 400 °C by plasma enhanced chemical vapor deposition (PECVD) [Park et al., 1996] or electron cycle resonance (ECR) deposition [Jeon et al., 1997]. However, these deposition techniques have difficulty in depositing void-free dielectrics over severe topography and also have the risk of radiation and particle generation during deposition.

Diethylsilane (DES) has recently gained attention as a new silicon source material suitable for low temperature deposition. Huo and Foo [1991] obtained high-quality SiO_2 films from DES and oxygen by a low pressure chemical vapor deposition (LPCVD) at low temperatures below 500 °C. They reported that the deposited films have a low residual carbon concentration less than about 1 % and the film conformality exceeds 83 %. Patterson and Ozturk [1992] observed in their experiments that there is a maximum in deposition rate at around 475 °C and copious amounts of SiO_2 particulates are generated at temperatures above 500 °C resulting in no deposition on the wafers. They also observed that below 0.55 torr the deposition rate is extremely small and above 0.95 torr ignition of the reactants in the gas phase occurs creating considerable SiO_2 particulates. Levy et al. [1993] showed that the deposition ceases abruptly for conditions where the total pressure is less than 0.35 torr or where the O_2/DES ratio is higher than 2.35. They obtained a poor uniformity across the wafer of about 20 %. Recently, Martin et al. [1995] performed studies of the gas-phase products, SiO_2 film properties, and kinetics of the DES/O_2 reaction. They found that reaction kinetics are first order in both DES and oxygen with an activation energy of about 29 kcal/mol. From their experimental results they concluded that the DES/O_2 reaction is achieved by a free radical mechanism.

In this work, we numerically investigate the LPCVD of SiO_2 films from DES and oxygen in a horizontal hot-wall reactor. We propose a new kinetic mechanism to explain the inversion maximum in deposition rate with increasing temperature, which is observed experimentally by Patterson and Ozturk [1992]. Deposition rate and film uniformity are studied over a wide range of operating conditions such as deposition temperature, pres-

†To whom correspondence should be addressed.
E-mail : ejkim@uou.ulsan.ac.kr

sure, reactant flow rate, and distance between the inlet and the wafer in an effort to optimize the DES/oxygen CVD process.

MODEL DEVELOPMENT

The mathematical model developed for the DES/oxygen LPCVD in the hot-wall reactor includes a set of partial differential equations with suitable boundary conditions describing fluid flow, heat transfer, and mass transport of chemical species. The present model involves chemical reactions both in the gas phase and on the wafer surface. Some simplifying assumptions can be applied to the CVD system considered in this work: (i) A steady state situation is considered; (ii) a laminar gas flow is assumed; (iii) the gas mixture is ideal; (iv) a continuum description of the gas is appropriate; and (v) heats of reactions are negligible. Energy contributions caused by chemical reactions may be neglected due to a low concentration of the reactants in the LPCVD system.

In the DES/O_2 LPCVD operations, the precursor, DES, is commonly introduced into the reactor without carrier gas. Furthermore, the O_2/DES ratio is typically maintained at 2. Therefore, the assumption of the precursor dilution in the gas, as adopted in most CVD modeling studies, is not applicable to the DES/O_2 CVD process.

With these assumptions, we have the governing equations that follow.

1. Governing Equations

In cylindrical coordinates the continuity equation is given by

$$\frac{1}{r}\frac{\partial(\rho r v)}{\partial r}+\frac{\partial(\rho u)}{\partial z}=0 \tag{1}$$

where ρ is the density of the gas mixture, u is the axial velocity, v is the radial velocity, r is the radial coordinate, and z is the axial coordinate.

The momentum equations governing the motion of the gas are written as

z-component:

$$\rho\left(v\frac{\partial u}{\partial r}+u\frac{\partial u}{\partial z}\right)=-\frac{\partial P}{\partial r}+\frac{1}{r}\frac{\partial}{\partial r}\left(\mu r\frac{\partial u}{\partial r}\right)+\frac{\partial}{\partial z}\left(\mu\frac{\partial u}{\partial z}\right) \tag{2}$$

r-component:

$$\rho\left(v\frac{\partial v}{\partial r}+u\frac{\partial v}{\partial z}\right)=-\frac{\partial P}{\partial r}+\frac{1}{r}\frac{\partial}{\partial r}\left(\mu r\frac{\partial v}{\partial r}\right)-\frac{\mu}{r^2}v+\frac{\partial}{\partial z}\left(\mu\frac{\partial v}{\partial z}\right) \tag{3}$$

where P is the pressure, and μ is the viscosity of the gas mixture.

The energy equation can be written as

$$\rho C_P\left(v\frac{\partial T}{\partial r}+u\frac{\partial T}{\partial z}\right)=\frac{1}{r}\frac{\partial}{\partial r}\left(kr\frac{\partial T}{\partial r}\right)+\frac{\partial}{\partial z}\left(k\frac{\partial T}{\partial z}\right) \tag{4}$$

where C_P and k are the heat capacity per unit mass and thermal conductivity of the gas mixture, respectively, and T is the temperature. We neglect viscous dissipation [Bird et al., 1960] and Dufour effects [Jenkinson and Pollard, 1984].

Finally, species balance equations take the form

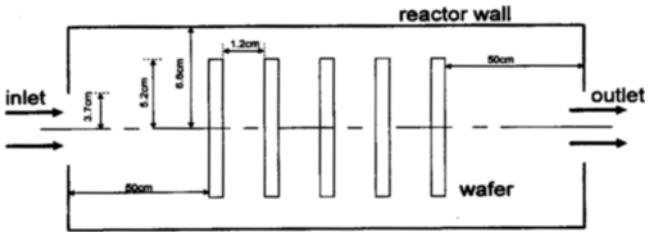

Fig. 1. Schematic diagram of the horizontal hot-wall reactor considered in this work.

$$C\left(v\frac{\partial x_i}{\partial r}+u\frac{\partial x_i}{\partial z}\right)=\frac{1}{r}\frac{\partial}{\partial r}\left(CD_i' r\frac{\partial x_i}{\partial r}\right)+\frac{\partial}{\partial z}\left(CD_i'\frac{\partial x_i}{\partial z}\right)+R_{g,i} \tag{5}$$

where C is the molar concentration of the gas, x_i is the mole fraction of species i, D_i' is the effective diffusion coefficient of species i in the gas mixture, and $R_{g,i}$ is the rate of formation of species i by gas phase reactions whose details are discussed in the Chemical Model section. The thermal diffusion is neglected in this work because there is no large temperature gradient in the hot-wall CVD reactor.

2. Boundary Conditions

We consider here a conventional horizontal hot-wall reactor whose configuration is depicted in Fig. 1. It is assumed that five wafers are placed in the reactor. The reactor is assumed to be axisymmetric, with no variations or velocity components in the angular direction. Boundary conditions on the above set of transport equations should be specified at the inlet, outlet, symmetric axis, reactor wall, and wafer surfaces.

The inlet boundary conditions are

$$u=u_{in},\ v=0,\ T=T_{in},\ Cux_{i,F}=Cux_i-CD_i'\frac{\partial x_i}{\partial z} \tag{6}$$

where u_{in} is the average inlet velocity, T_{in} is the inlet temperature, $x_{i,F}$ is the mole fraction of species i in the feed. Danckwerts' conditions are used for the species balance [Danckwerts, 1953]. At the outlet, a zero normal gradient condition is applied for all dependent variables.

$$\frac{\partial u}{\partial z}=0,\ \frac{\partial v}{\partial z}=0,\ \frac{\partial T}{\partial z}=0,\ \frac{\partial x_i}{\partial z}=0 \tag{7}$$

Since the reactor is considered to be axisymmetric, the centerline conditions are

$$\frac{\partial u}{\partial r}=0,\ v=0,\ \frac{\partial T}{\partial r}=0,\ \frac{\partial x_i}{\partial r}=0 \tag{8}$$

On the reactor wall and wafer surface, the normal and tangential velocities are zero and the temperature is maintained at T_w. We assume that SiO_2 films are deposited both on the wafer surface and on the reactor wall.

$$u=0,\ v=0,\ T=T_w,\ CD_i'\frac{\partial x_i}{\partial n}=-R_{s,i} \tag{9}$$

where n denotes the unit normal outward vector to the surface of the solid, and $R_{s,i}$ is the rate of formation of species i by surface reactions.

3. Transport Properties of Gas Species

The physical properties appearing in the governing equa-

tions are a function of temperature, pressure, and composition. The ideal gas law is used as an equation of state

$$\rho = \frac{PM_w}{RT} \tag{10}$$

where R is the gas constant, and M_w is the molecular weight of the gas mixture that is given as

$$M_w = \sum_i x_i M_i \tag{11}$$

where M_i is the molecular weight of species i. Viscosities of pure components are calculated from the Chapman-Enskog equation derived from the molecular theory

$$\mu_i = 2.6693 \times 10^{-5} \frac{\sqrt{M_i T}}{\sigma^2 \Omega_\mu} \tag{12}$$

where μ_i is the viscosity of species i in $gcm^{-1}s^{-1}$, σ is the collision diameter in Å, and Ω_μ is a collision integral that is calculated by the equation proposed by Neufeld et al. [1972]

$$\Omega_\mu = \frac{A}{T^{*B}} + \frac{C}{e^{DT^*}} + \frac{E}{e^{FT^*}} \tag{13}$$

where A=1.16145, B=0.14874, C=0.52487, D=0.77320, E=2.16178, F=2.43787, and $T^*=\kappa T/\varepsilon$. Here ε is a characteristic energy interaction between molecules and κ is the Boltzmann constant. Lennard-Jones parameters for each species are listed in Table 1. Multicomponent viscosities are obtained by Wilke's approximation [Bird et al., 1960]

$$\mu_{mix} = \sum_i \frac{x_i \mu_i}{\sum_j x_j \Phi_{ij}} \tag{14}$$

where

$$\Phi_{ij} = \frac{1}{\sqrt{8}} \left(1 + \frac{M_i}{M_j}\right)^{-1/2} \left[1 + \left(\frac{\mu_i}{\mu_j}\right)^{1/2} \left(\frac{M_j}{M_i}\right)^{1/4}\right]^2 \tag{15}$$

The thermal conductivity of the gas mixture may be estimated by a method analogous to that given for viscosity

Table 1. Lennard-Jones parameters

Species	σ (Å)	ε/κ (K)
DES	6.278	476.5
O_2	3.433	113.0
DESONE	6.354	603.5
Ethylene	4.232	205.0
H_2O	2.641	809.1

$$k_{mix} = \sum_i \frac{x_i k_i}{\sum_j x_j \Phi_{ij}} \tag{16}$$

where k_i is the thermal conductivity of the pure component that is given by the Eucken equation [Bird et al., 1960]

$$k_i = \left(C_{P,i} + \frac{5}{4}\frac{R}{M_i}\mu_i\right) \tag{17}$$

The heat capacity of the mixture is calculated from

$$C_P = \sum_i \omega_i C_{P,i} \tag{18}$$

where ω_i is the mass fraction of species i, and $C_{P,i}$ is the heat capacity of species i in $calg^{-1}K^{-1}$ that is a function of temperature given as

$$C_{P,i} = a_i + b_i T + c_i T^2 + d_i T^3 \tag{19}$$

The values of the constants for each species in Eq. (19) are given in Table 2. The constants for DES and diethylsilanone (DESONE) are estimated by using the Joback group contribution method. Binary diffusivities can be calculated from the Chapman-Enskog equation

$$D_{ij} = 0.0018583 \frac{\sqrt{T^3\left(\frac{1}{M_i} + \frac{1}{M_j}\right)}}{P\sigma_{ij}^2 \Omega_D} \tag{20}$$

in which D_{ij} is the binary diffusivity in cm^2s^{-1}, T is in K, P is in atm, and σ_{ij} is in Å. Here

$$\sigma_{ij} = (\sigma_i + \sigma_j)/2 \tag{21}$$

$$\varepsilon_{ij} = (\varepsilon_i \varepsilon_j)^{1/2} \tag{22}$$

Diffusion collision integral Ω_D is calculated by the equation proposed by Neufeld et al. [1972]

$$\Omega_D = \frac{A'}{T^{*B'}} + \frac{C'}{e^{D'T^*}} + \frac{E'}{e^{F'T^*}} + \frac{G'}{e^{H'T^*}} \tag{23}$$

where A'=1.06036, B'=0.15610, C'=0.19300, D'=0.47635, E'=1.03587, F'=1.52996, G'=1.76474, and H'=3.89411. The diffusion of species i in a multicomponent mixture is written in the form of Fick's law of diffusion with an effective diffusion coefficient D_i' that is given by

$$D_i' = \left(1 - \frac{M_w \omega_i}{M_i}\right)\left(\sum_{j \neq i} \frac{M_w \omega_j}{M_j D_{ij}}\right)^{-1} \tag{24}$$

Table 2. Values of the constants appearing in Eq. (19)

Species	a_i	b_i	c_i	d_i
DES	1.033×10^{-1}	7.495×10^{-4}	6.353×10^{-7}	-6.029×10^{-10}
O_2	1.902×10^{-1}	1.134×10^{-4}	-5.341×10^{-8}	9.791×10^{-12}
DESONE	1.051×10^{-1}	6.927×10^{-4}	5.781×10^{-7}	-5.620×10^{-10}
Ethylene	3.243×10^{-2}	1.334×10^{-3}	-7.112×10^{-7}	1.496×10^{-10}
H_2O	4.276×10^{-1}	2.552×10^{-5}	1.400×10^{-7}	-4.770×10^{-11}

4. Chemical Model

Even though several studies on the DES/O_2 CVD have been reported in the literature, its deposition mechanism is not yet understood well. Based on the observations made by Patterson and Ozturk [1992] and Martin et al. [1995] we propose a new simple kinetic mechanism for DES/oxygen CVD: DES decomposes to intermediate species in the gas phase when colliding with oxygen. We assume DESONE, $(C_2H_5)_2Si{=}O$, as a strong candidate for the intermediate as Martin et al. [1995] speculated. The presence of another intermediate other than the one proposed here does not affect our model significantly. Some of the intermediate molecules decompose completely to SiO_2 in the gas phase before they reach the wafer surface. Undecomposed intermediate molecules adsorb on the wafer surface. They then react with two adjacent adsorbed oxygen atoms to yield SiO_2 films, which is assumed to be the rate-limiting step. We assume that the oxygen molecule dissociates upon adsorption with each oxygen atom occupying one vacant site. The deposition of SiO_2 films is inhibited by gas products such as ethylene and water. However, it is found that the inhibition effect is not crucial in the present analysis because the pressure considered is very low. Details of deposition mechanism for the DES/O_2 CVD proposed here are given as

Gas phase

$$DES + O_2 \xrightarrow{k_1} DESONE + H_2O \tag{25}$$

$$DESONE + O_2 \xrightarrow{k_2} SiO_2 + 2C_2H_4 + H_2O \tag{26}$$

Surface

$$DESONE\ (g) + * \xleftrightarrow{K_{DESONE}} DESONE\ (a) \tag{27}$$

$$O_2(g) + 2* \xleftrightarrow{K_{O_2}} 2O\ (a) \tag{28}$$

$$C_2H_4\ (g) + * \xleftrightarrow{K_{ETH}} C_2H_4\ (a) \tag{29}$$

$$H_2O\ (g) + * \xleftrightarrow{K_{H_2O}} H_2O\ (a) \tag{30}$$

$$DESONE\ (a) + 2O\ (a) \xrightarrow{k_3} SiO_2\ (s) + 2C_2H_4\ (a) + H_2O\ (a) \tag{31}$$

With the mechanism above, one can determine the detailed rate expressions for the gas-phase and surface reactions as follows:

Gas phase

$$R_{g,DES} = -k_1 C_{DES} C_{O_2} \tag{32}$$

$$R_{g,DESONE} = k_1 C_{DES} C_{O_2} - k_2 C_{DESONE} C_{O_2} \tag{33}$$

$$R_{g,O_2} = -k_1 C_{DES} C_{O_2} - k_2 C_{DESONE} C_{O_2} \tag{34}$$

$$R_{g,ETH} = 2k_2 C_{DESONE} C_{O_2} \tag{35}$$

Surface

$$R_d = \frac{k_r C_{DESONE} C_{O_2}}{(1+K_{O_2}^{1/2} C_{O_2}^{1/2} + K_{DESONE} C_{DESONE} + K_{ETH} C_{ETH} + K_{H_2O} C_{H_2O})^3} \tag{36}$$

where $k_r = k_3 K_{DESONE} K_{O_2}$. Maeda and Nakamura [1981] determined the adsorption equilibrium constants for oxygen and silane by fitting the experimental data with the rate expression they proposed.

$$K_{O_2} = 4.7 \times 10^{-3} e^{7,000/RT},\ mol^{-1}cm^3 \tag{37}$$

$$K_{SIL} = 2.0 \times 10^{-3} e^{9,500/RT},\ mol^{-1}cm^3 \tag{38}$$

Haupfear et al. [1994] obtained from their experiments where the temperature ranges from 770 to 1,000 °C the value of the adsorption constant for ethylene as

$$K_{ETH} = 8.48 \times 10^{-3} e^{20,300/RT},\ torr^{-1} \tag{39}$$

However, the order of magnitude of the adsorption constant in Eq. (39) becomes unreasonably large in the temperature range considered in this work where the temperature is maintained below 500 °C. In addition, there is no data available on the adsorption constants for water and DESONE. Therefore, we use here the adsorption constant of oxygen for water and ethylene, and that of silane for DESONE as an approximation. It is found that a variation in the value of the adsorption constant does not significantly change the predicted results.

5. Method of Solution

To solve numerically the above set of governing equations along with boundary conditions in two-dimensional cylindrical coordinates, we employ in this work a control-volume-based finite difference method. The computational domain is divided into a non-uniform array of control volumes which are made smaller in the wafer region. We use a staggered grid system in which the velocity components are stored midway between adjacent grid nodes while all the other variables are stored at the grid nodes.

The differential equations are integrated over discrete control volumes to generate the discretized equations. A power-law scheme is employed to evaluate the convection-diffusion fluxes. Since the discretized equations resulting are coupled and nonlinear, an iterative method is required. The discretized algebraic equations are evaluated by using a line-by-line tridiagonal-matrix algorithm (TDMA). The velocity field is first obtained from the discretized momentum equations in the z and r directions, employing the SIMPLER (semi-implicit method for pressure-linked equations-revised) algorithm [Patankar, 1980]. The energy equation is then solved to obtain the temperature field. Finally, the species balance equations are solved based on velocity and temperature fields obtained. The iterative procedure is followed until a satisfactory convergence is achieved. The residuals of the equations are typically less than 10^{-5} after 500 iterations. All calculations are carried out on a Solbourne computer (Axil 311).

RESULTS AND DISCUSSION

The mathematical model described previously is used to investigate the LPCVD of SiO_2 films from DES/O_2 in the hot-wall horizontal reactor depicted in Fig. 1. We consider here that five wafers are placed in the middle of the reactor. The computational domain typically consists of 140 grid cells (6 grid cells in the interwafer region) in the axial direction and

20 grid cells in the radial direction. To check the cell independence of the results, calculations are also made on a 280×40 cell for one representative situation. The calculated deposition rates on the fine cell are found to differ less than 1% from those obtained on the standard cell. It is also found that there is no virtual difference in deposition rate and film uniformity between wafers except for the 1st wafer.

In this work, the experimental results reported by Patterson and Ozturk [1992] are used to determine the reaction rate constants appearing in Eqs. (32) to (36) and are compared with the model predictions. The base conditions for the present analysis are the following: DES/O_2 ratio=2, total flow rate=300 sccm, deposition pressure=0.75 torr, wafer temperature=450 °C, inlet temperature=60 °C, reactor diameter=13 cm, distance between the inlet and the wafer=50 cm. These conditions are based on experimental conditions given by Patterson and Ozturk [1992]. The wall temperatures at both ends of the chamber are assumed to be 60 °C. In Fig. 2, predicted streamline, temperature, and concentration distributions are shown for base conditions. The indicated values in Fig 2(b) are the temperatures in K and in Fig. 2(c)-(e) mole fractions. It can be seen in Fig. 2(b) that the variations in the temperature take place only in the region near the inlet and outlet. As shown in Fig. 2(c)-(e), the concentrations vary more rapidly in the upstream region and are uniform over the wafer. One can also see in Fig. 2 that DES and O_2 concentrations decrease as one proceeds along the reactor whereas intermediate species, DESONE, concentration increases.

Rate constants for gas-phase and surface reactions are determined by using an iterative method to match the predicted deposition rates from the model with experimental data.

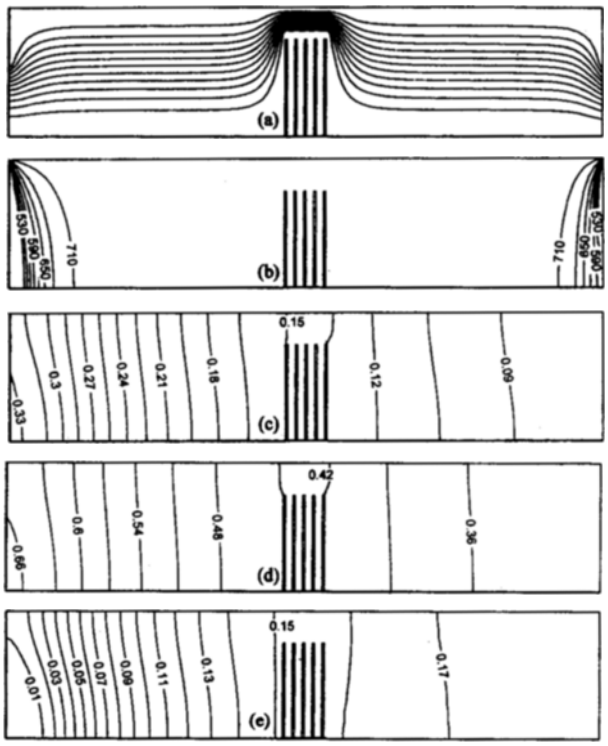

Fig. 2. Computed contours of (a) streamline, (b) temperature, (c) DES concentration, (d) oxygen concentration, (e) DESONE concentration for base conditions.

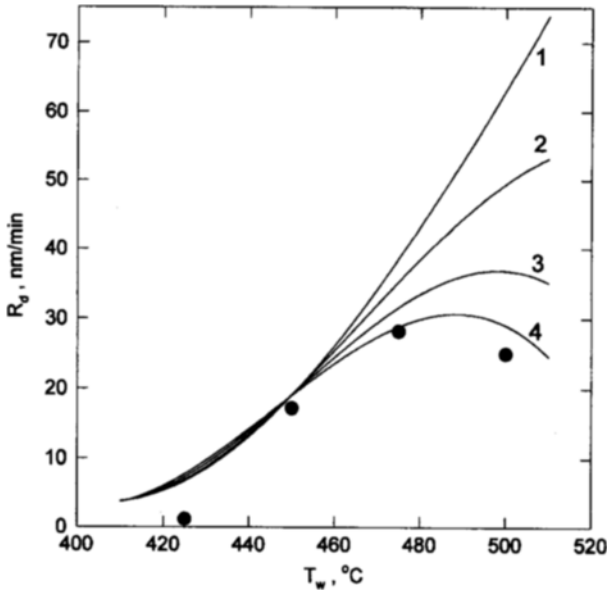

Fig. 3. Deposition rate as a function of wafer temperature. P=0.75 torr, F_t=300 sccm, O_2/DES=2. Experimental data (●) from Patterson and Qzturk [1992]. Numerical predictions; solid lines 1: E_a=30,000 cal/mol, 2: E_a=40,000 cal/mol, 3: E_a=50,000 cal/mol, 4: E_a=57,000 cal/mol

$$k_1 = 1.36\times10^{17}e^{-29,100/RT},\ \text{mol}^{-1}\text{cm}^3\text{s}^{-1} \quad (40)$$

$$k_2 = 1.43\times10^{25}e^{-57,000/RT},\ \text{mol}^{-1}\text{cm}^3\text{s}^{-1} \quad (41)$$

$$k_r = 1.31\times10^{19}e^{-35,000/RT},\ \text{mol}^{-1}\text{cm}^4\text{s}^{-1} \quad (42)$$

Here the value of the rate constant for DES decomposition reaction, k_1, is identical to that obtained by Martin et al. [1995].

Fig. 3 illustrates the deposition rate as a function of wafer temperature. Here the pressure is 0.75 torr, the total flow rate is 300 sccm, and the O_2/DES ratio is 2. Experimental data show that the rate of deposition of the SiO_2 films increases up to 475 °C, at which a maximum occurs, and the rate decreases above the level. The predicted results show that if the activation energies for the DESONE decomposition reaction are less than 50,000 cal/mol, the deposition rate increases rapidly with increasing temperature even at wafer temperatures above 475 °C. It is seen in Fig. 3 that as the activation energy is increased, the deposition rate reduces enormously at higher wafer temperatures. The predictions with the activation energy for the DESONE decomposition reaction of 57,000 cal/mol, line 4, are found to be in good agreement with experiments. The numerical results, lines 1 and 2, with activation energies of 30,000 and 40,000 cal/mol, respectively, do not properly explain the experimental trend. The high activation energy for DESONE decomposition reaction implies that DESONE decomposition reaction, i.e., parasitic gas-phase reaction, becomes more significant at higher temperatures. The activation energy for the surface reaction can be evaluated from the data taken at temperatures below 475 °C, where parasitic gas-phase reaction may not be considerable. As seen in Fig. 3, the model successfully describes the experimental data and shows clearly that the deposition rate of the DES/O_2 LPCVD process is

limited by parasitic gas-phase reaction, not mass transfer in the gas phase, nor surface adsorption of the reactants; this causes a decrease in the rate of deposition. Patterson and Ozturk [1992] observed in their experiments that plentiful amounts of SiO_2 particulates are generated in the gas phase above 500 °C resulting in no deposition on the wafers, which supports our kinetic mechanism involving parasitic gas-phase reactions. It should be mentioned that further improvements in the accuracy of the reaction constants may be achieved through systematic experiments combined with the present method of analysis.

The deposition rate as a function of pressure at 450 °C is shown in Fig. 4, where the total flow rate is 300 sccm, and the O_2/DES ratio is 2. The predictions show that at pressures below 0.5 torr the deposition rate is decreased rapidly as the pressure is reduced. Patterson and Ozturk [1992] reported that the deposition rate obtained is extremely small below 0.55 torr. Levy et al. [1993] also observed in their experiments that the deposition rate is not measurable at pressures less than 0.35 torr. The reason for this appears to be that the frequency of collisions with activating species decreases rapidly at very low pressures. The experimental data of Levy et al. [1993] in Fig. 4 are taken at F_t=150 sccm and T_w=400 °C. As shown in Fig. 4, our model predicts experimental trend reasonably well.

The good agreement between the predictions from the model developed in this work and the experimental deposition rate data available from the literature enables us to perform a systematic study of the influence of process conditions to get a deeper insight in the effects of these variables on film growth rate and uniformity. As mentioned above, deposition rate and concentration profiles on the wafer surface are virtually identical for all the wafers except for the 1st wafer. Over the range of operating conditions considered in this work, the 1st wafer is found to have extremely uniform concentration and deposition rate profiles possibly due to a stagnation point flow over it, yielding uniform momentum and concentration boundary layers on it. Predicted deposition rates and concentrations on the wafer surface shown hereafter in the figures are for the 3rd wafer.

Fig. 5 illustrates the influence of wafer temperature on deposition rate at pressures varying from 0.5 to 1.0 torr. It can be seen that the temperature, at which the inversion in the deposition rate occurs, decreases as the pressure increases. This inversion becomes pronounced as the pressure is increased from 0.5 to 1.0 torr indicating that the parasitic gas-phase reactions become more significant with increasing pressure. In Fig. 6

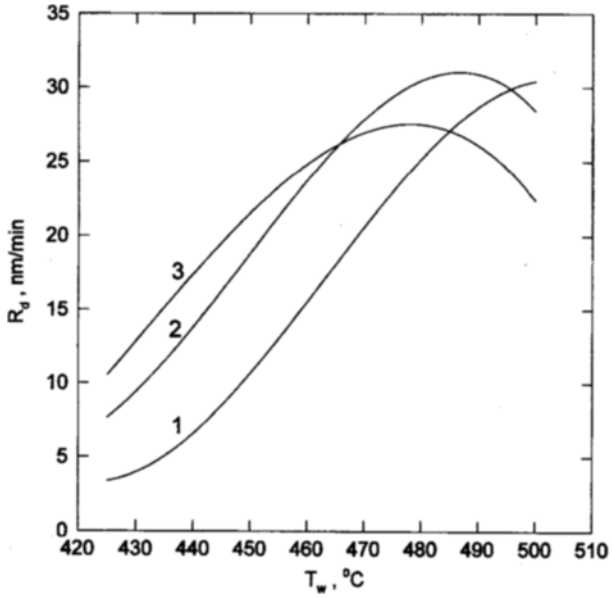

Fig. 5. Influence of wafer temperature on deposition rate at various pressures.
F_t=300 sccm, O_2/DES=2. Line 1: P=0.5 torr, 2: P=0.75 torr, 3: P=1.0 torr

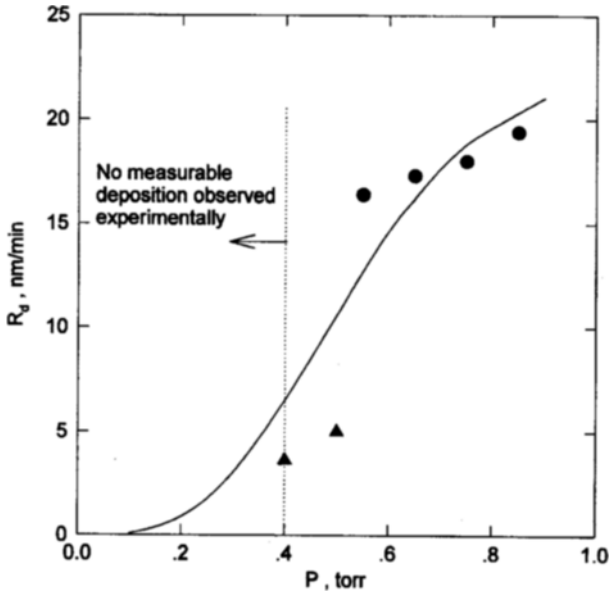

Fig. 4. Deposition rate as a function of pressure.
T_w=450 °C, F_t=300 sccm, O_2/DES=2. Experimental data (●) by Patterson and Ozturk [1992], (▲) by Levy et al. [1993]. Numerical predictions are solid lines.

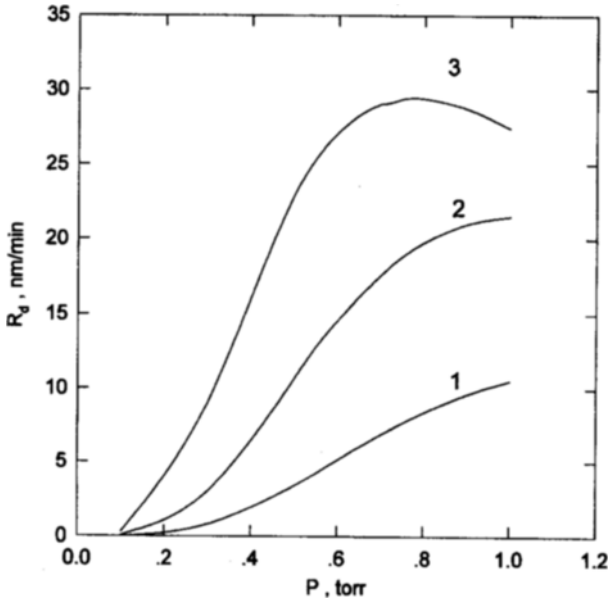

Fig. 6. Influence of pressure on deposition rate at various wafer temperatures.
F_t=300 sccm, O_2/DES=2. Line 1: T_w=425 °C, 2: T_w=450 °C, 3: T_w=475 °C

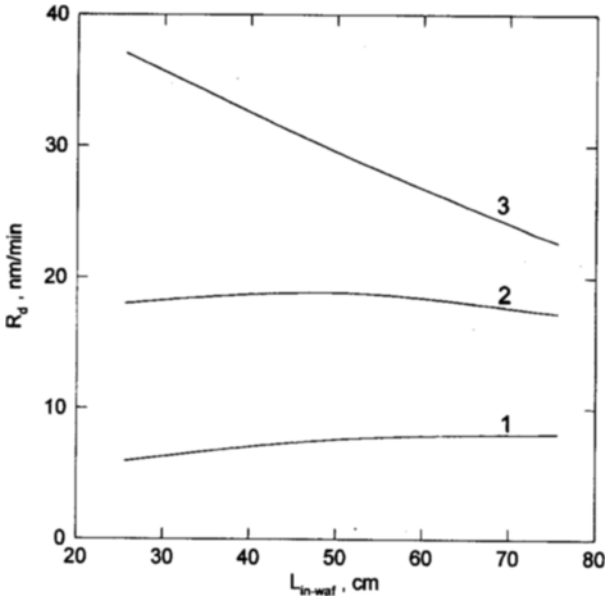

Fig. 7. Influence of distance between the inlet and the first wafer on deposition rate at various wafer temperatures.
P=0.75 torr, F_t=300 sccm, O_2/DES=2. Line 1 : T_w=425 °C, 2 : T_w=450 °C, 3 : T_w=475 °C

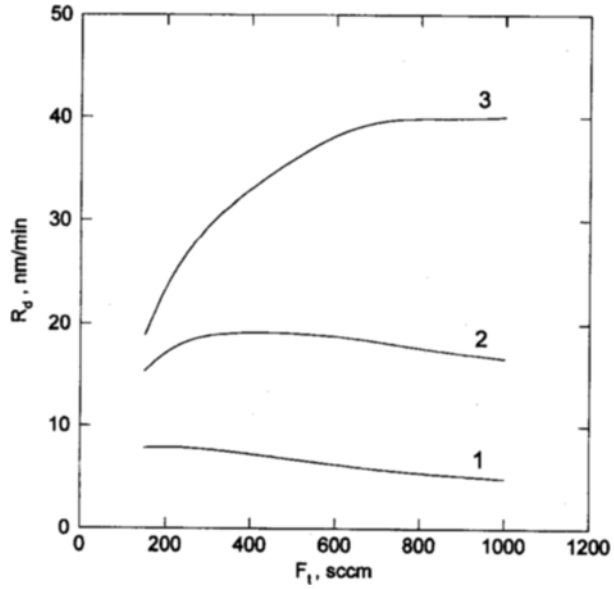

Fig. 8. Influence of total flow rate on deposition rate at various wafer temperatures.
P=0.75 torr, O_2/DES=2. Line 1 : T_w=425 °C, 2 : T_w=450 °C, 3 : T_w=475 °C

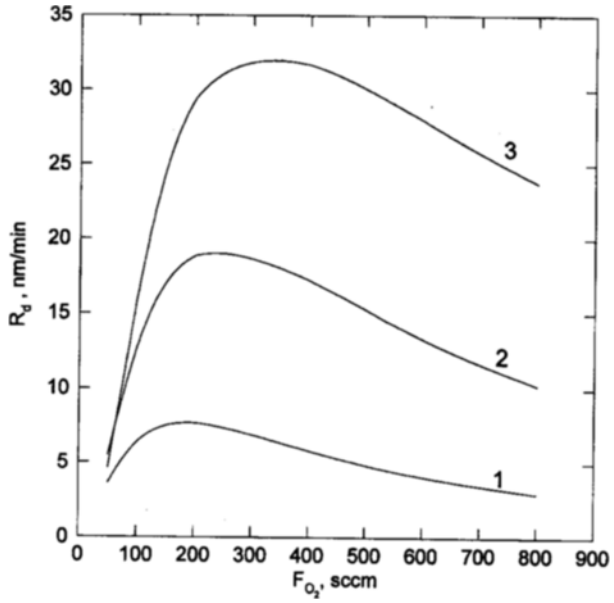

Fig. 9. Influence of oxygen flow rate on deposition rate at various wafer temperatures.
P=0.75 torr, F_{DES}=100 sccm. Line 1 : T_w=425 °C, 2 : T_w=450 °C, 3 : T_w=475 °C

the deposition rate is plotted as a function of pressure at temperatures ranging from 425 to 475 °C. One can see that at temperatures below 475 °C the deposition rate increases monotonically with increasing pressure, but at 475 °C there is a maximum in deposition rate at around 0.7 torr.

The effect of distance between the inlet and the wafer on deposition rate at temperatures ranging from 425 to 475 °C is illustrated in Fig. 7. It is interesting to note that at low temperatures, say 425 °C, the deposition rate increases slightly as the distance increases, whereas at high temperatures, say 475 °C, it decreases considerably with increasing distance. The reason for this behavior may be that as the distance increases, the residence time of the molecules in the reactor increases for a given flow rate. At low temperatures where parasitic gas-phase reactions are not significant, more molecules of intermediate species are produced in the gas phase as the distance increases, and this results in an increase in the deposition rate. However, at high temperatures where parasitic gas-phase reactions are significant, an increase in the distance depletes intermediate species in the gas phase. This causes a decrease in the deposition rate at high temperatures. The effect of parasitic gas-phase reaction is also shown in Fig. 8, where the deposition rate is plotted against the total flow rate. It is seen that at a low temperature of 425 °C, the deposition rate decreases slightly as the total flow rate increases, whereas at an elevated temperature of 475 °C, it increases considerably with increasing total flow rate up to about 600 sccm, and becomes saturated above the level. At low temperatures, as the total flow rate increases, fewer molecules of intermediate species are produced in the gas phase due to reduced residence time; this results in a decrease in the deposition rate. However, at high temperatures, an increase in the total flow rate suppresses parasitic gas-phase reactions thus generating more intermediate species. This causes an increase in the deposition rate at high temperatures. Fig. 9 shows the predicted results of the effect of oxygen flow rate on deposition rate for a given DES flow rate of 100 sccm. It is seen that the deposition rate increases rapidly as the oxygen flow rate increases up to 200-300 sccm, at which the deposition rate becomes a maximum, then it decreases significantly with a further increase in oxygen flow rate. Levy et al. [1993] observed that the deposition rate decreases sharply at high O_2/DES ratios above 2. This may be because the para-

sitic gas-phase reactions become pronounced with increasing oxygen flow rate.

Film uniformity as well as deposition rate is an important performance measure. In order to obtain uniform deposition, both the reactant concentration and the temperature should be uniform over the wafer surface as Eq. (36) indicates. In Fig. 10(a) the influence of pressure on the variation in DESONE concentration above the wafer surface is depicted. We find higher DESONE concentrations at the wafer edge than at the wafer center. DESONE molecules are decomposed mainly in the gas phase. As the gas diffuses from the wafer edge to the wafer center, the DESONE concentration decreases because the DESONE decomposition rate exceeds its formation rate at a temperature of 475 °C where parasitic-gas phase reaction is significant. However, we found that the pattern of the DESONE concentration profile across the wafer depends on the level of pressure and temperature. At temperatures below 450 °C and pressures below 0.5 torr, where parasitic gas-phase reactions are not significant, the DESONE decomposition rate is lower than its formation rate. In this case, as one moves from the wafer edge to the wafer center, more DESONE molecules are generated resulting in higher DESONE concentration at the wafer center. Fig. 10(b) shows the influence of pressure on the variation in oxygen concentration above the wafer surface. One can see that the oxygen concentration is decreased as one goes from the wafer edge to the wafer center. DES is found to have the same pattern of concentration profile as oxygen. As is clearly to be expected, the oxygen concentration is decreased more rapidly as the pressure is increased. Fig. 10(c) illustrates the influence of pressure on the film uniformity over the wafer. It is seen that the film uniformity is improved as the pressure is decreased. Fig. 11 shows the influence of wafer temperature on the film uniformity over the wafer. We see that the film uniformity can be improved as the wafer temperature is decreased from 500 to 425 °C; however, the deposition rate is reduced simultaneously. Therefore, at higher wafer temperatures one obtains a high deposition rate at the expense of the film uniformity. The influence of total flow rate on the film uniformity over the wafer is illustrated in Fig. 12. Here the O_2/DES ratio is fixed at 2. One can see that the film uniformity is improved as the total flow rate is increased from 300 to 1,000 sccm. This may be because the convective mass transfer is enhanced with increasing flow rate. Therefore, high total flow rates of around 1,000 sccm would be desirable for obtaining both high deposition rate and good uniformity. However, as the total flow rate is increased, keeping DES concentration fixed, more DES is consumed. The influence of DES flow rate on the film growth uniformity over the wafer is depicted in Fig. 13 in which the oxygen flow rate is held at 200 sccm. It is seen that the film uniformity is improved as the DES flow rate is increased from 50 to 400 sccm. In Fig. 14 the influence of oxygen flow rate on the film uniformity over the wafer is shown at a given DES flow rate of 100 sccm. One can see that as the O_2 flow rate is increased from 100 to 600 sccm, the film uniformity is lowered. Accordingly, oxygen has a different effect on film uniformity than DES. As seen above in Fig. 9, above 300 sccm the deposition rate is decreased significantly with increasing O_2 flow rate. Therefore, oxygen flow rates high-

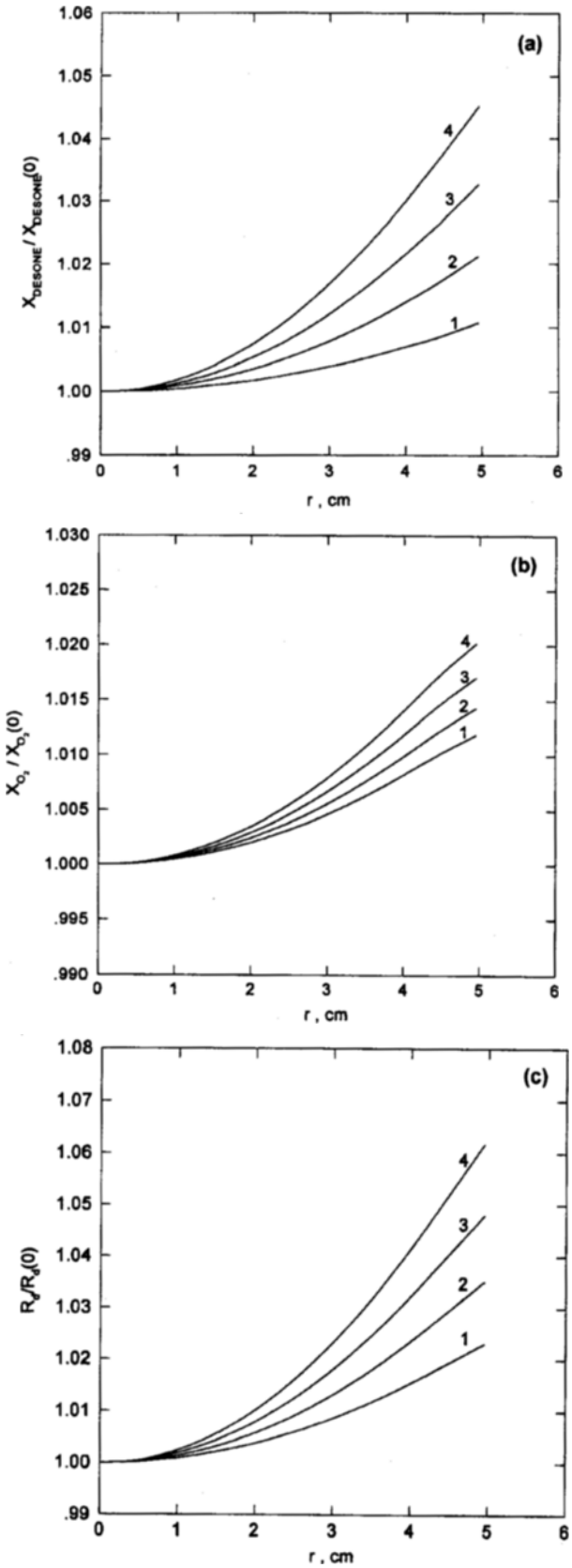

Fig. 10. Influence of pressure on the radial variation in (a) DESONE concentration, (b) oxygen concentration, (c) deposition rate above the wafer surface.
T_w=475 °C, F_t=300 sccm, O_2/DES=2. Line 1 : P=0.5 torr, 2 : P=0.6 torr, 3 : P=0.75 torr, 4 : P=1.0 torr

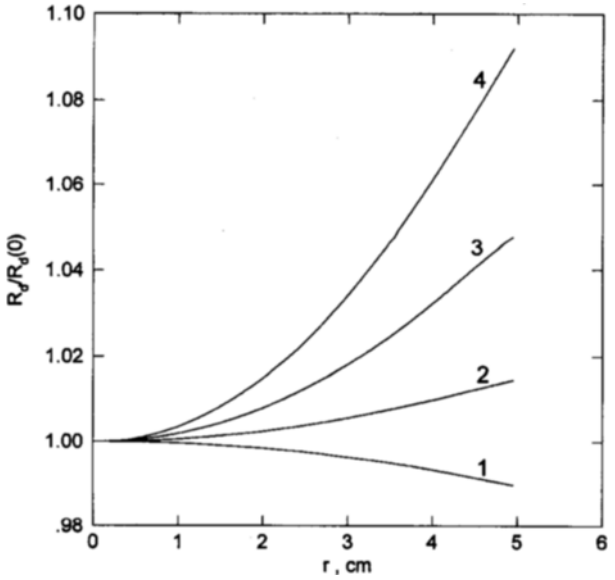

Fig. 11. Influence of wafer temperature of the film uniformity. P=0.75 torr, F_t=300 sccm, O_2/DES=2 Line 1 : T_w=425 °C, 2 : T_w=450 °C, 3 : T_w=475 °C, T_w=500 °C

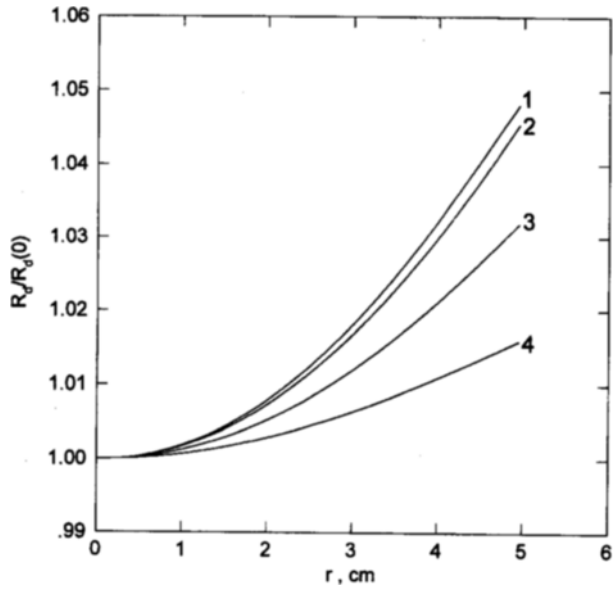

Fig. 12. Influence of total flow rate on the film uniformity. P=0.75 torr, T_w=475 °C, O_2/DES=2 Line 1 : F_t=300 sccm, 2 : F_t=600 sccm, 3 : F_t=800 sccm, 4 : F_t=1,000 sccm

er than 300 sccm may cause less uniform films as well as lower deposition rates.

CONCLUSION

A mathematical model has been developed for the LPCVD of SiO_2 films from DES/O_2 in a horizontal hot-wall reactor. A new kinetic mechanism that includes parasitic gas-phase reactions is proposed to explain the inversion maximum in deposition rate with increasing temperature. The reaction constants associated with the kinetic mechanism proposed are determined by matching the simulated results with the experimental data

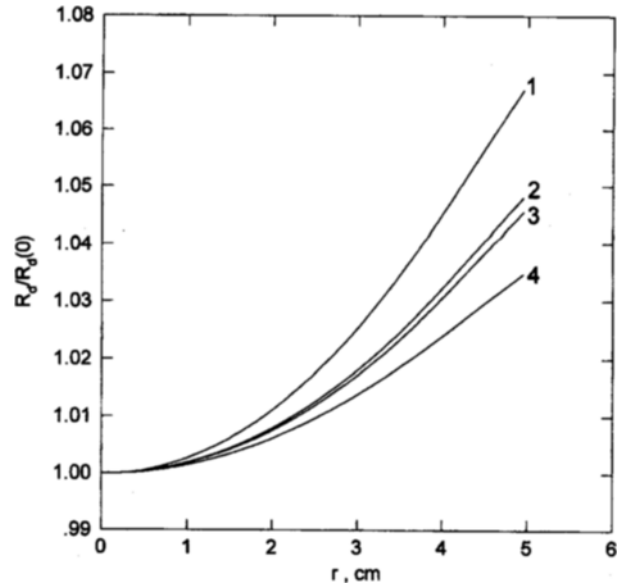

Fig. 13. Influence of DES flow rate on the film uniformity. P=0.75 torr, T_w=475 °C, F_{O2}=200 sccm. Line 1 : F_{DES}=50 sccm, 2 : F_{DES}=100 sccm, 3 : F_{DES}=200 sccm, 4 : F_t=400 sccm

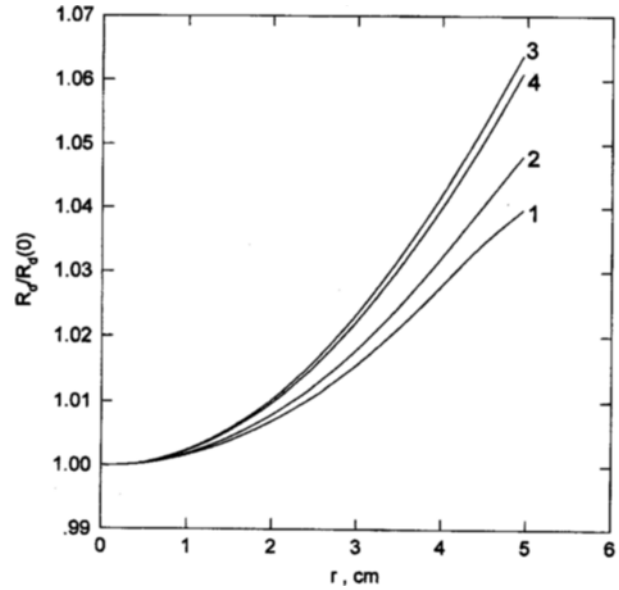

Fig. 14. Influence of oxygen flow rate on the film uniformity. P=0.75 torr, T_w=475 °C, F_{DES}=100 sccm. Line 1 : F_{O2}=100 sccm, 2 : F_{O2}=200 sccm, 3 : F_{O2}=400 sccm, 4 : F_{O2}=600 sccm

available. The model is found to explain successfully the trend of the experimental data.

Parasitic gas-phase reactions become increasingly important as the pressure and temperature are increased. As the wafer temperature is increased up to 475 °C, the deposition rate is increased at the expense of the film uniformity. Above 475 °C, the deposition rate is decreased with a further increase in temperature due to parasitic gas-phase reactions. As the pressure is reduced, the film uniformity is improved. The deposition rate becomes a maximum at a pressure of around 0.75 torr. The O_2/DES ratio of around 2.5 provides a maximum in deposi-

tion rate. The predictions show that a total flow rate of 1,000 sccm, a pressure of 0.75 torr, and a temperature of 475 °C are preferable for obtaining both high deposition rate and good film uniformity.

ACKNOWLEDGMENT

This work was supported financially by the University of Ulsan under a 1995 University Research Grant.

NOMENCLATURE

- C : gas concentration [mol/cm^3]
- C_p : heat capacity of the gas [cal/g-K]
- D_i : diffusion coefficient of species i [cm^2/s]
- D_i' : effective diffusion coefficient of species i [cm^2/s]
- k : thermal conductivity of the gas [cal/cm-K]
- K_i : adsorption equilibrium constant of species i [cm^3/mol]
- k_{sub} : reaction rate constant, units vary (sub refers to appropriate subscript)
- M_i : molecular weight of species i [g/mol]
- M_w : average molecular weight of gas mixture [g/mol]
- n : unit normal outward vector to the surface [cm]
- P : absolute pressure [dyne/cm^2]
- r : radial position as measured from the center [cm]
- R : gas constant [=1.987 cal/mol-K]
- R_d : rate of SiO_2 film deposition [mol/cm^2-s]
- $R_{g,i}$: rate of formation of species i by gas-phase reactions [mol/cm^3-s]
- $R_{s,i}$: rate of formation of species i by surface reactions [mol/cm^2-s]
- T : absolute temperature [K]
- T^* : dimensionless temperature [$=\kappa T/\varepsilon$]
- T_{in} : inlet temperature [K]
- T_w : wafer temperature [K]
- u : axial velocity [cm/s]
- u_{in} : inlet velocity [cm/s]
- v : radial velocity [cm/s]
- x_i : mole fraction of species i
- $x_{i,F}$: mole fraction of species i in the feed
- z : axial position as measured from the inlet [cm]

Greek Letters

- ε : characteristic energy of interaction between molecules [erg]
- κ : Boltzmann constant [$=1.3805\times10^{-16}$ erg/K]
- μ : gas viscosity [g/cm-s]
- ρ : gas density [g/cm^3]
- σ : collision diameter [A]
- ω_i : mass fraction of species i
- Ω_D : diffusion collision integral in Eq. (23)
- Ω_μ : viscosity collision integral in Eq. (13)

REFERENCE

Bird, R. B., Stewart, W. E. and Lightfoot, E. N., "Transport Phenomena," John Wiley & Sons, Inc., New York (1960).

Haupfer, E. A., Olson, E. C. and Schmidt, L. D., "Kinetics of SiO_2 Deposition from Tetraethylorthosilicate," *J. Electrochem. Soc.*, **141**, 1943 (1994).

Huo, D. T. C., Yan, M. F. and Foo, P. D., "SiO_2 Films by Low Pressure Chemical Vapor Deposition Using Diethylsilane: Processing and Characterization," *J. Vac. Sci. Technol. A*, **9**, 2602 (1991).

Jenkinson, J. P. and Pollard, R., "Thermal Diffusion Effects in Chemical Vapor Deposition Reactors," *J. Electrochem. Soc.*, **131**, 2911 (1984).

Jeon, B.-J., Oh, I.-H., Lim, T.-H. and Jung, I.-H., "Characteristics of Silicon Oxide Films Prepared by Chemical Vapor Deposition Using ECR Plasma Source," *HWAHAK KONGHAK*, **35**, 374 (1997).

Levy, R. A., Grow, J. M. and Chakravarthy, G. S., "Low-Pressure Chemical Vapor Deposition of Silicon Dioxide Using Diethylsilane," *Chem. Mater.*, **5**, 1710 (1993).

Maeda, M. and Nakamura, H., "Deposition Kinetics of SiO_2 Film," *J. Appl. Phys.*, **52**, 6651 (1981).

Martin, J. G., O'Neal, H. E. and Ring, M. A., "Mechanisms of Silicon Dioxide Deposition from the Low Pressure Chemical Vapor Deposition of Diethylsilane/Oxygen Mixtures," *J. Electrochem. Soc.*, **142**, 3873 (1995).

Neufeld, P. D., Jansen, A. R. and Aziz, R. A., "Empirical Equations to Calculate 16 of the Transport Collision Integral $\Omega^{(l,s)^*}$ for the Lennard-Jones (12-6) Potential," *J. Chem. Phys.*, **57**, 1100 (1972).

Park, Y.-B., Kang, J.-K. and Rhee, S.-W., "Remote Plasma Chemical Vapor Deposition (RPCVD) of Low Temperature Silicon Oxide," *HWAHAK KONGHAK*, **34**, 143 (1996).

Patterson, J. D. and Ozturk, M. C., "Low Pressure Chemical Vapor Deposition of Silicon Dioxide below 500 °C by the Pyrolysis of Diethylsilane in Oxygen," *J. Vac. Sci. Technol. B*, **10**, 625 (1992).

Reid, R. C., Prausnitz, J. M. and Poling, B. E., "The Properties of Gases & Liquids," 4th Ed., McGraw-Hill, New York (1987).